# 2004 Indian Ocean tsunami flow velocity measurements from survivor videos

Hermann M. Fritz,[1] Jose C. Borrero,[2] Costas E. Synolakis,[2,3] and Jeseon Yoo[1]

Received 2 May 2006; revised 2 October 2006; accepted 15 November 2006; published 19 December 2006.

[1] The tsunami of 26th December 2004 severely affected Banda Aceh along the North tip of Sumatra (Indonesia) at a distance of 250 km from the epicenter of the magnitude 9.0 earthquake. This tsunami flow velocity analysis focused on two survivor videos recorded within Banda Aceh more than 3 km from the open ocean. The exact locations of the tsunami eyewitness video recordings were revisited by the survey team between February 22 and 25, 2005 to record camera calibration ground control points. The motion of the camera during the recordings was determined. The individual video images were rectified with a direct linear transformation (DLT) assuming a planar water surface at the level. Finally a cross-correlation based particle image velocimetry (PIV) analysis was applied to the rectified video images to determine instantaneous tsunami flow velocity fields. The measured tsunami flow velocities were within the range of 2 to 5 m/s. **Citation:** Fritz, H. M., J. C. Borrero, C. E. Synolakis, and J. Yoo (2006), 2004 Indian Ocean tsunami flow velocity measurements from survivor videos, *Geophys. Res. Lett.*, *33*, L24605, doi:10.1029/2006GL026784.

## 1. Introduction

[2] On December 26th at 00:58:53 UTC, a great earthquake with a moment magnitude of 9.0 – or possibly greater [*Stein and Okal*, 2005] – occurred 250 km southwest of the North tip of Sumatra, Indonesia. Large tsunamis were generated and severely damaged coastal communities in countries along the Indian Ocean, including Indonesia, Thailand, Sri Lanka, India, Maldives and Somalia resulting in the loss of more than 200,000 human lives [*Synolakis and Bernard*, 2006; *Synolakis and Kong*, 2006; *Titov et al.*, 2005]. In the near field of the epicenter the North and West Coasts of Sumatra were hardest hit by the tsunami [*Borrero*, 2005a]. In the far field the tsunami severely affected Sri Lanka westward across the Bay of Bengal at a distance of 1600 km from the epicenter [*Liu et al.*, 2005]. The Maldives were over washed an hour after Sri Lanka at a distance of 2500 km from the epicenter [*Fritz et al.*, 2006]. In East Africa the tsunami impact focused on Somalia some 5000 kilometers to the west of the earthquake epicenter [*Fritz and Borrero*, 2006].

[1]School of Civil and Environmental Engineering, Georgia Institute of Technology, Savannah, Georgia, USA.
[2]Department of Civil Engineering, University of Southern California, Los Angeles, California, USA.
[3]Also at Department of Environmental Engineering, Technical University of Crete, Chania, Greece.


0094-8276/06/2006GL026784

## 2. Post Tsunami Field Surveys

[3] Several tsunami reconnaissance trips were conducted to Sumatra including Banda Aceh [*Borrero et al.*, 2006]. A combination of standard tsunami field survey techniques [*Synolakis and Okal*, 2005] were used. Tsunami run-up and flow depth measurements were collected primarily between January 4 and 9, 2005 [*Borrero*, 2005b]. This report focuses solely on the revisit of tsunami eyewitness video recording locations in Banda Aceh between February 22 and 25, 2005 and the subsequent video image calibration, processing and tsunami flow velocity analysis. The two video recordings were precisely located by comparing perspective views of features and landmarks in the background of the videos [*Borrero et al.*, 2006]. The two video recording locations are: location (A) near the grand mosque in downtown Banda Aceh and location (B) in a residential area southwest of the city center. The locations (A) and (B) are 3 and 3.5 km in southeastern direction from the open ocean and 4.2 km apart parallel to the shore. The Camera man positions and viewing sectors are located on post tsunami satellite images (Figure 1). Location A is surrounded by city blocks of mainly intact houses. The transition from intact main frames to houses with washed out walls, partial collapses and total destruction occurred between 200 and 400 m closer to the shore westwards of location A. Location B is in a damage transition zone with a large percentage of buildings destroyed.

[4] Panorama A of Figure 2 is the post tsunami view from the camera man's position on the southwest corner of the grand mosque; the encircling wall shows the street intersection and corner buildings present in the eyewitness tsunami video. Location A is characterized by buildings with intact main frames and limited flood damage. Location B: the view during the survey from the camera man position on the second story balcony of a residential home in the flood plain shows the significant destruction at site B with many buildings razed to the ground (Figure 2). Even the remaining well built structures exhibit significant wash out damage primarily on the first floor.

## 3. Eyewitness Video Camera Calibration

[5] The calibration of the sector of view present in the eyewitness video recordings is of critical importance in order to extract quantitative tsunami flow velocity information. The camera calibration task was complicated by the fact that the recordings were shot with handheld amateur video cameras by survivors under extreme stress. The videos exhibited significant camera motions while following the tsunami. The camera man rotation induced significant translations in subsequent video images, whereas tilting in subsequent video images was limited. Recording sequences with visible lens zooming were not analyzed. The

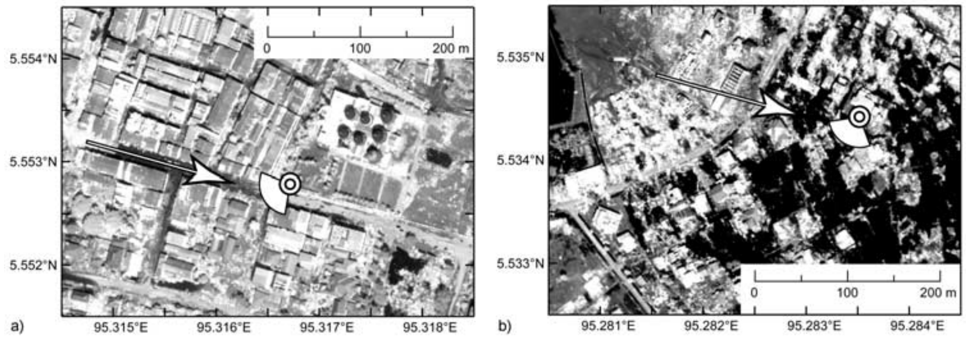


**Figure 1.** Camera man positions (circles), angles of view (sectors) and tsunami impact directions (→) on post tsunami Quickbird-satellite images of the video image recording areas: (a) location A: grand mosque southwest corner of encircling wall, (b) location B: 2nd story balcony of residential home in flood plane (acquisition date 28-Dec-2004; resolution 0.6 m/pixel panchromatic band).

amateur video camera models remained unknown and therefore intrinsic camera parameters such as lens distortions were not compensated. The photogrammetric transformation between the 3-D world and 2-D image coordinates requires the input of both the world coordinates (3-D space) and the image coordinates (2-D plane) of visually identifiable ground control points. Large parts of the eyewitness videos images cover the tsunami flow itself with fixed objects in the background and peripheral parts of the images. The limited number of objects suitable for ground control points in tsunami inundation videos introduced additional difficulties. The survey team measured most suitable ground control points with a laser range finder with integrated digital inclinometer and compass (Laser-Craft Contour XLRic).

## 4. Camera Motion Analysis With PIV

[6] The video image motion induced by the panning of the video camera was determined from subsequent raw color images by means of planar particle image velocimetry (PIV). PIV is an image window cross-correlation based measurement technique which uses multiple images of flow tracing patterns in a confined plane to measure the two in-plane velocity components simultaneously throughout the area of interest [*Raffel et al.*, 1998]. Prior to the PIV-analysis the steady image areas such as houses sticking out of the tsunami were isolated from the rest of the image with digital masks. The video images are considered as planar images during the entire analysis process. The images were processed with a 8-bit grayscale intensity depth. The instantaneous planar displacement fields are computed with a cross-correlation based adaptive multi-pass algorithm, which builds around a basic spatial cross-correlation function $R_{II}$ in its discrete form

$$R_{II}(\Delta x, \Delta y) = \frac{1}{p^2} \sum_{i=0}^{p-1} \sum_{j=0}^{p-1} I_1(i,j) I_2(i + \Delta x, j + \Delta y) \qquad (1)$$

for $p \times p$ pixel interrogation windows, where $I_1$ and $I_2$ are matrix intensity functions from corresponding interrogation windows. The correlation plane for displacements $\Delta x$ and $\Delta_y$ within $\pm p/2$ is not computed directly but via a much faster standard cyclic FFT-based algorithm [*Raffel et al.*, 1998]. The cross-correlation function $R_{II}$ of the two

**Figure 2.** Post-tsunami panorama views of the sectors in the eyewitness video recordings from the camera man positions: (a) location A: downtown street corner southwest of grand mosque, (b) location B: 2nd story balcony of residential home in flood plane.

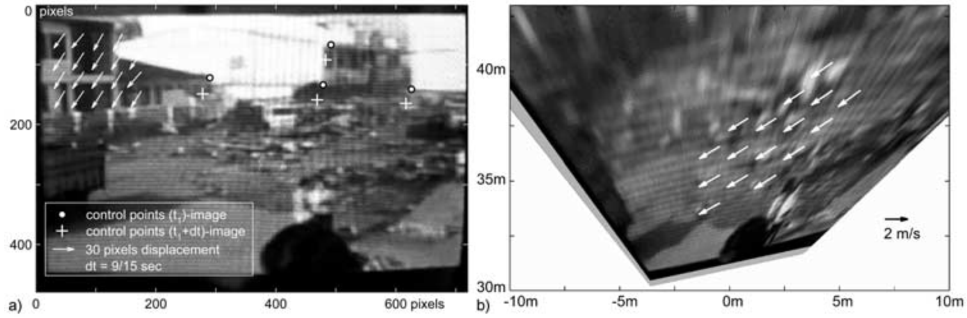


**Figure 3.** A1 (Location A, sequence 1): approaching tsunami front: (a) raw video image with selected ground control points and computed camera motion, (b) rectified video image with computed instantaneous tsunami flow velocity vector field.

intensity functions $I_1$ and $I_2$ is equivalent to a complex conjugate multiplication of their Fourier transforms.

$$R_{II} \Leftrightarrow \hat{I}_1 \cdot \hat{I}_2^* \quad (2)$$

where $\hat{I}_1$ and $\hat{I}_2$ are the Fourier transforms of the matrix intensity functions $I_1$ and $I_2$ respectively, and $\hat{I}_2^*$ is the complex conjugate of $\hat{I}_2$. The fractional part of the displacement is determined by interpolation of the correlation peak. The adaptive multi-pass algorithm first calculated a reference displacement field from the double image input. A standard cross-correlation interrogation was performed with a relatively large interrogation window size (256 $\times$ 256 pixels). The calculated displacement field was used as reference displacement field for the next higher resolution level. The iteration was repeated until the final window size (64 $\times$ 64 pixels) was reached. The second pass at the final window size was conducted with 50% window offsets and window deformations. In this manner the window shift is adaptively improved to compute the displacements with iteratively refined interrogation windows. The computed camera displacements at location A exceeded 20 pixels in several sequences (Figures 3a and 4a) and was less than 1 pixel in other cases (Figure 5a), while at location B it exceeded 20 pixels (Figure 6a). The mean camera translation was determined with a bi-linear regression in the planar coordinates. The exact determination of the camera motion was of crucial importance since in some cases the camera motion was on the same order of magnitude as tsunami flow velocity.

## 5. Video Image Rectification

[7] The transformation of the raw tsunami video images from image coordinates to world coordinates preceded the PIV tsunami flow velocity analysis to avoid any physical distortion. Herein, in order to transform the video frame coordinates to real world coordinates, the Direct Linear Transformation (DLT) method was applied [*Holland et al.*, 1997]. The DLT coefficients are linearized parameters of the collinear relationship between each image coordinates and its corresponding world coordinates. The DLT coefficients are determined from the ground control points by using a least squares method. Between 9 and 11 ground control points were used in the tsunami video image calibration process, which is well above the absolute minimum of 6 ground control points. The applied linear relationship between image and world coordinates was

$$i = \frac{L_1 x + L_2 y + L_3 z + L_4}{L_9 x + L_{10} y + L_{11} z + 1}, \quad j = \frac{L_5 x + L_6 y + L_7 z + L_8}{L_9 x + L_{10} y + L_{11} z + 1} \quad (3)$$

where $(i, j)$ = image pixel coordinates; $(x, y, z)$ = real world coordinates; $L_k$ $(k = 1, \cdots, 11)$ = the DLT coefficients. Using equation 5 given with the pre-determined DLT coefficients, the transformation of image coordinates to world coordinates was applied by constraining the elevation $z$ in real coordinates to the measured tsunami surface. This was

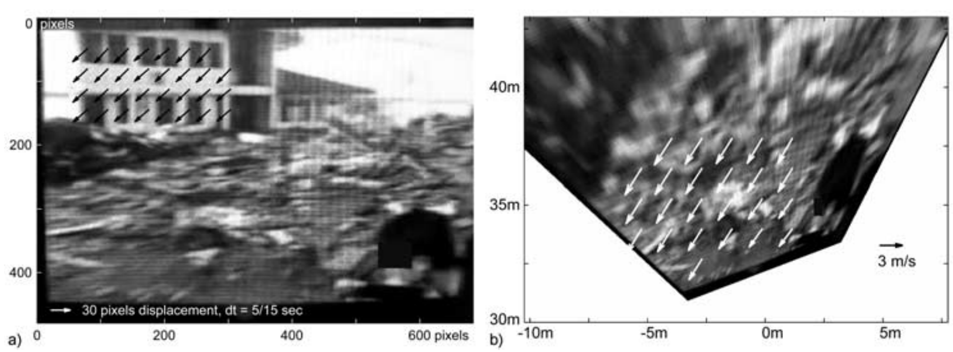


**Figure 4.** A2: tsunami flooding with flow depth $h$ = 1.2 m: (a) raw video image with computed camera motion, (b) rectified video image with computed tsunami flow velocity vector field.

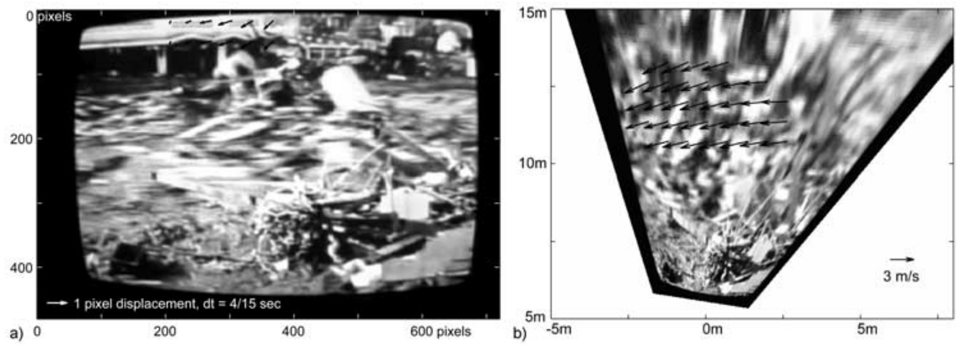


**Figure 5.** A3: tsunami flooding with flow depth $h$ = 1.3 m: (a) raw video image (with negligible camera motion <1 pixel) viewing from the sidewall across the street perpendicular to the tsunami flow, (b) rectified video image with computed tsunami flow velocity vector field.

required because the system of equations is underdetermined (two equations with three unknowns). This assumption limits the transformation to a planar tsunami surface and neglects local surface elevation features. The tsunami video images were rectified accordingly and resampled to convert the rectified images onto a regular pixel matrix. Thereby the pixel resolution was increased to 0.02 m/pixel avoiding artifacts due to the image rectification process. Rectified tsunami video image maps form the background of the tsunami flow velocity vector fields (Figures 3b, 4b, 5b, and 6b). The significantly oblique viewing angles and the wide camera angles of view caused the massive distortions of the raw video images during the rectification process. In the raw video recordings flow tracers close to the camera misleadingly appear to be moving at least 3 times as fast as flow tracers further away from the camera although the tsunami flow velocities were widely uniform at time steps.

## 6. Tsunami Flow Velocity Analysis With PIV

[8] Finally, the digital PIV analysis method discussed under the section on the camera motion was applied to the rectified tsunami video images. The tsunami surface during flooding through Banda Aceh was characterized by a debris like flow resulting in non-discrete image patterns. In previous studies the PIV method was successfully applied to granular landslide surfaces with non-discrete image patterns [*Fritz*, 2002] as well as near shore flow structures in the swash zone [*Holland et al.*, 2001]. Similarly, herein we applied the cross-correlation based PIV analysis to subsequent tsunami inundation images resulting in instantaneous tsunami velocity vector fields. The velocity vector components $u$ and $v$ in the image space domain were computed by equation 4 with the window displacements $\Delta x$ and $\Delta y$ determined from the correlation plane and the image acquisition settings given by the time interval $\Delta t$.

$$u = \frac{\Delta x}{\Delta t}, \; v = \frac{\Delta y}{\Delta t} \tag{4}$$

The adaptive multi-pass algorithm first calculates a reference vector field from the double image input. A standard cross-correlation interrogation is performed with a relatively large interrogation window size (256 × 256 pixels) and a mean initial window shift. The calculated vector field is used as reference vector field for the next higher resolution level. The previous interrogation window size is refined after each iteration. The iteration is repeated until the final window size (128 × 128 or 64 × 64 pixels) is reached. Spurious velocity vectors were removed based on the ratio between the first and second peak in the correlation plane (a so called Q-factor). The calculated window displacements ranged from 40 to 80 pixels, which corresponds to 0.8 to 1.6 m in physical space based on the rectified image resolution of 0.02 m/pixel. The corresponding time intervals between two images inserted into the PIV-analysis varied between 0.26s to 0.60s. These time intervals were selected based on optimized signal-to-noise ratios. In

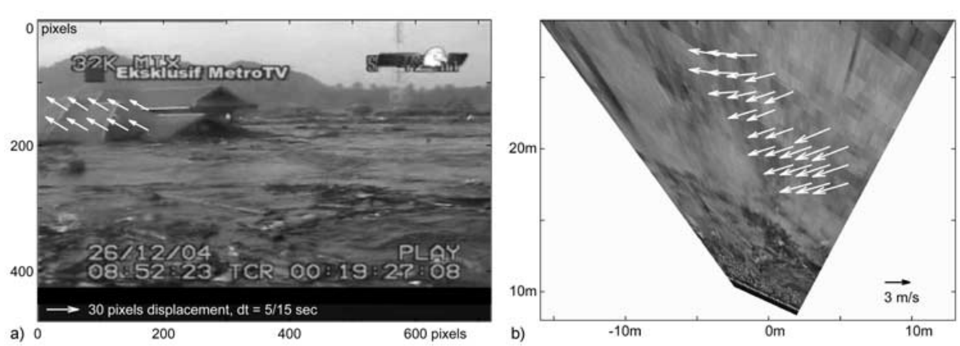


**Figure 6.** Location B: tsunami flooding with flow depth $h$ = 4 m: (a) raw video image with computed camera motion, (b) rectified video image with computed tsunami flow velocity vector field.

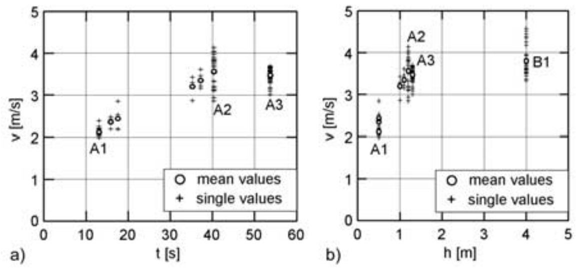


**Figure 7.** Measured tsunami flow velocities: (a) time series at location A, (b) flow velocities versus flow depths at locations A and B.

some cases the camera motion reached up to 30 pixels over the same time interval corresponding to 75% of the tsunami flow velocity vector. This illustrates the importance of subtracting the camera motion prior to the tsunami flow velocity analysis. Instantaneous flow velocity fields are presented for three cases (A1, A2 and A3) at location A (Figures 3b, 4b, and 5b) and one case (B1) at location B (Figure 6b). The eyewitness video recording at location A started with the appearance of the tsunami front in the field of view. The 7 tsunami flow velocity vector fields determined at location A span the first minute of the recording. The velocity time series at location A indicates that the tsunami front velocity was rapidly exceeded with increasing flow depth (Figure 7). The tsunami flow velocity at location A roughly doubled within 25s, which lead to misjudgments of the tsunami flow velocity by victims simply looking at the initially slow approaching tsunami front in awe or walking slowly at the pace of the front velocity. The accumulated measurement errors are estimated to plus/minus 20% from the scattering of individual data points assuming a homogenous flow field in the measurement area. The Froude-numbers $F = v/\sqrt{gh}$ for the different cases were computed to $F_{A1} = 0.95, F_{A2} = 1.04, F_{A3} = 0.97$ and $F_{B1} = 0.61$. The tsunami overland flow at location A was characterized by standing surface waves confirming the transcritical flow regime with $F = 1$ [*Fritz and Hager*, 1998]. The video recording at location B showed a later stage of the tsunami inundation with flow depths of several meters and smooth water surfaces indicating a subcritical flow regime ($F < 1$). This was confirmed by the computed Froude-number $F_{B1} = 0.61$.

## 7. Conclusions

[9] The rapid response of the survey team to Banda Aceh after the December 26th, 2004 catastrophic event led to the recovery of important data on the characteristics of the tsunami effects and inundation of a major city in the tsunami near field. The analysis focused on two survivor videos recorded within Banda Aceh more than 3 km from the open ocean. The revisit of the exact locations of the tsunami eyewitness video recordings and the calibration of the camera fields of view from the perspective of the camera man was imperative for the extraction of quantitative information from tsunami survivor videos. The motion of the camera during the recordings was determined with a cross-correlation based particle image velocimetry (PIV) applied to masked steady areas of the images. The direct linear transformation (DLT) successfully rectified the perspective video images based on the ground control points measured during the survey, thereby assuming a planar water surface at the level of the mean water surface at each time step. Finally the PIV-analysis was applied to the rectified video images to determine instantaneous tsunami flow velocity fields. The measured tsunami flow velocities were within the range of 2 to 5 m/s, which corresponds to less than half the flooding velocities estimated without accounting for perspective viewing [*Borrero et al.*, 2006]. The flow velocities increased with increasing flow depths in the analyzed video time series. This lead to the misjudgment of the tsunami flooding velocity by victims comforted by the walking velocity of the approaching tsunami front not realizing that 40s after the appearance of the tsunami front the tsunami flooding reached running speeds of 4 m/s (15 km/h).

[10] **Acknowledgments.** The survey team was supported by the National Science Foundation, the German National Television ZDF, and several UN-Organizations operating in Banda Aceh in February 2005.

## References

Borrero, J. C. (2005a), Field data and satellite imagery of tsunami effects in Banda Aceh, *Science*, *308*(5728), 1596.
Borrero, J. C. (2005b), Field survey of northern Sumatra and Banda Aceh, Indonesia after the tsunami and earthquake of 26 December 2004, *Seismol. Res. Lett.*, *76*, 312–320.
Borrero, J. C., C. E. Synolakis, and H. M. Fritz (2006), Field surveys of northern Sumatra after the tsunami and earthquake of 26 December 2004, *Earthquake Spectra*, *22*(S3), S93–S104.
Fritz, H. M. (2002), PIV applied to landslide generated impulse waves, in *Laser Techniques for Fluid Mechanics*, edited by R. J. Adrian et al., pp. 305–320, Springer, New York.
Fritz, H. M., and J. C. Borrero (2006), Somalia field survey of the 2004 Indian Ocean tsunami, *Earthquake Spectra*, *22*(S3), S219–S233.
Fritz, H. M., and W. H. Hager (1998), Hydraulics of embankment weirs, *J. Hydraul. Eng.*, *124*(9), 963–971.
Fritz, H. M., C. E. Synolakis, and B. G. McAdoo (2006), Maldives field survey of the 2004 Indian Ocean tsunami, *Earthquake Spectra*, *22*(S3), S137–S154.
Holland, K. T., R. A. Holman, and T. C. Lippmann (1997), Practical use of video imagery in nearshore oceanographic field studies, *IEEE J. Oceanic Eng.*, *22*(1), 81–92.
Holland, K. T., J. A. Puleo, and T. N. Kooney (2001), Quantification of swash flows using video-based particle image velocimetry, *Coastal Eng.*, *44*, 65–77.
Liu, P. L.-F., P. Lynett, J. Fernando, B. E. Jaffe, H. M. Fritz, B. Higman, R. Morton, J. Goff, and C. E. Synolakis (2005), Observations by the International Tsunami Survey Team in Sri Lanka, *Science*, *308*(5728), 1595.
Raffel, M., C. E. Willert, and J. Kompenhans (1998), *Particle Image Velocimetry-A Practical Guide*, Springer, New York.
Stein, S., and E. A. Okal (2005), Size and speed of the Sumatra earthquake, *Nature*, *434*, 580–582.
Synolakis, C. E., and E. A. Okal (2005), 1992–2002: Perspective on a decade of post-tsunami surveys, *Adv. Nat. Technol. Haz.*, *23*, 1–30.
Synolakis, C. E., and E. N. Bernard (2006), Tsunami Science before and after Boxing Day 2004, *Phil. Trans. R. Soc.*, A364, 2231–2265.
Synolakis, C. E., and L. Kong (2006), Run up measurements of the December 2004 tsunami, *Earthquake Spectra*, *22*(53), 567–591.
Titov, V. V., A. B. Rabinovich, H. O. Mofjeld, R. E. Thomson, and F. I. González (2005), The global reach of the 26 December 2004 Sumatra tsunami, *Science*, *309*(5743), 2045–2048.

J. C. Borrero and C. E. Synolakis, Department of Civil Engineering, University of Southern California, Los Angeles, CA 90089, USA. (jborrero@usc.edu; costas@usc.edu)
H. M. Fritz (corresponding author) and J. Yoo, School of Civil and Environmental Engineering, Georgia Institute of Technology, Savannah, GA 31407, USA. (fritz@ gatech.edu)